Supplemental Information

Head swivel on the ribosome facilitates translocation via intra-subunit tRNA hybrid sites

Andreas H. Ratje, Justus Loerke, Aleksandra Mikolajka, Matthias Brünner,Peter W. Hildebrand, Agata L. Starosta, Alexandra Dönhöfer, Sean R. Connell, Paola Fucini, Thorsten Mielke, Paul C. Whitford, Jose' N Onuchic, Yanan Yu, Karissa Y. Sanbonmatsu, Roland K. Hartmann, Pawel A. Penczek, Daniel N. Wilson, and Christian M.T. Spahn

Supplemental Results and Discussion

Molecular structures of sub-states I (TI^PRE) and II (TI^POST)

In order to generate pseudo-atomic models for sub-states I (TI^{PRE}) and II (TI^{POST}) we employed the MDFIT method to flexibly dock the X-ray structure of the 70S ribosome in complex with EF-G[1] into the cryo-EM density maps. The resulting models fit the density well (**Fig. 1**). In order to quantify the fit, we calculated FSC curves between our final cryo-EM maps and density derived from the corresponding atomic coordinates (**supp. Fig. S2**). The 0.5 cutoff of these FSC curves for the TI^{PRE} and TI^{POST} is at 8.0 Å and 7.5 Å, respectively, and thus comparable to the nominal resolution of the cryo-EM maps. Nevertheless, it is important to note that the resolution of the map is in the sub-nanometer range and therefore, small, local changes in the model are not necessarily reliable. Thus, it is reassuring that the pseudo-atomic models contain large-scale conformational changes of the ribosomes (intersubunit rotation, head swivel, movement of the L1 protuberance and the stalk base region) but are locally very close to the X-ray structures of the *T. thermophilus* ribosome[1,2]. For example the root mean square deviation (r.m.s.d.) values of the phosphate atoms for the main body of the 23S rRNA between the X-ray structure of the POST 70S•EF-G complex[1] and the TI^{PRE} and TI^{POST} are only 0.9 Å and 0.7 Å, respectively. This appears to be negligible compared to the nominal resolution of 7.6 - 7.8 Å of the cryo-EM maps. Also the head domains and the body/platform domains of the 30S subunits are locally essentially unchanged as reflected by r.m.s.d. values for the 16S rRNA of 1.0 – 1.1 Å. Only the comparison of the head domains of the POST 70S•EF-G complex[1] and the TI^{POST} gives a slightly elevated r.m.s.d. value of 1.7 Å for the respective 16S rRNA phosphate atoms. As this value can be reduced to 1.1 Å when nucleotides 930-1044 constituting the 30S beak are left out for the comparison, there may be some smaller rearrangement of this region in addition to the large swivel movement of the head.

The MDFIT method essentially resulted in a rigid body fit for EF-G for both the TI^{PRE} and the TI^{POST} maps, i.e. the conformation of EF-G was hardly changed compared to the X-ray structure of the POST 70S•EF-G complex[1]. In contrast, significant changes can be observed for the tRNA structure present in the TI^{PRE} and the TI^{POST} complexes. The phosphate atoms of residues 2-72 of the tRNA have an r.m.s.d. value of 3.4 Å when the P-site tRNA of the POST 70S•EF-G complex[1] is compared with the pp/E tRNA of the TI^{PRE} and comparison with the pe/E tRNA of the TI^{POST} produces a r.m.s.d. value of 2.2 Å. The difference to the E-site tRNA of the POST 70S•EF-G complex[1] is even larger, as revealed by r.m.s.d. values of 4.6 Å when compared to either the pp/E tRNA of the TI^{PRE} or the pe/E tRNA of the TI^{POST}. Although the pp/E and the pe/E tRNA are different in conformation to the

classical P and E site tRNAs, they appear to be quite similar when compared with one other (r.m.s.d. value of 1.5 Å). Thus, the tRNA likely moves essentially as a rigid body during the partial translocation from the pp/E site of the TI[PRE] to the pe/E site of the TI[POST] (**Supp. Mov 1-4**). This tRNA movement can be described as a pivot at the CCA end, which is bound to its binding site on the 50S E-site. The L1 protuberance contacts the elbow of the tRNA in both states and has shifted to an intermediate position in the TI[POST] to accommodate the tRNA movement (**supp. Fig. S4**).

The conformational change of the pp/E tRNA and the pe/E tRNA relative to the structure of the classical P tRNA can be described by a kink at the junction of the anticodon stem and the D stem (**Fig. 2d**) since the tRNA models align very well at the acceptor stem, D-stem loop and T-stem loop (r.m.s.d. values of 0.8 Å and 0.9 Å for the pp/E-tRNA and pe/E-tRNA, respectively). As in the case of the A/T tRNA[3], the pp/E and pe/E tRNAs are bent at the junction between D stem and anticodon stem, however, they bend in the opposite direction (**Fig. 2d**). Compared to the structure of the classical P-tRNA the kink in the pp/E-tRNA and the pe/E-tRNA moves the anticodon region by about 11-12 Å towards the E-site region. Thus, the conformational change present in both the pp/E- and pe/E-tRNAs suggests an active role for tRNA during the translocation step.

Structure of FA-stalled EF-G

The structures of EF-G•GDP•FA appear identical or at least very similar in both the TI[PRE] and the TI[POST] (**Fig. 1; supp. Fig. S7**). Compared to the structures of vacant EF-G•GDP[4-6], the fusidic acid stalled EF-G adopts an opened-up conformation [7,8] where domains IV and V are moved as a rigid body relative to domains I and II. Furthermore, domain III is found rotated independently of domains IV and V. Thus, the overall structure of EF-G is essentially identical to our previous sub-nanometer resolution cryo-EM structure of ribosome-bound EF-G•GMPPNP[9] and to the recent X-ray structure of EF-G•GDP•FA bound to the POST 70S ribosome[1] (**Fig. 3a**). It is remarkable that the overall domain arrangement of ribosome-bound EF-G is hardly influenced by the ratchet-like subunit rearrangement (RSR) of the ribosome. However, in contrast to the structure of ribosome-bound EF-G•GMPPNP[9], we do not observe density for the switch 1 region of EF-G in the GTP state position. Instead, we observe some unassigned, fragmented density close to helix 14 of 16S rRNA. Thus, in agreement with biochemical data[10] and similar to kirromycin-stalled EF-Tu[3,11], the switch 1 region is likely to be in a dynamic, partially disordered state. It is not even clear if there is a defined GDP conformation for the switch 1 region of EF-G since it is disordered in X-ray structures of vacant EF-G[4-6] as well as in the recent X-ray structure of EF-G•GDP•FA bound to the POST 70S ribosome[1].

The switch 1 region of EF-G in the GTP state links domains I and III by non-covalent interactions and has therefore been implicated in the conformational rearrangement of domain III of EF-G[9]. Although the switch 1 region of EF-G appears disordered in the present EF-G•GDP•FA, there is density connecting domains I and III close to the position of the switch 1 region in the GTP state (**supp. Fig. S7**). As this additional density is surrounded by EF-G residues implicated in FA binding[4,12], we tentatively assigned this density to FA. In order to corroborate this assignment, we searched for potential small molecule-binding sites on EF-G using Ligsite[13], a tool for predicting protein binding sites. Using default parameters (a grid space of 1.0Å, a probe radius of at least 5.0Å), one of the two most probable binding locations for FA falls right into the cryo-EM density between EF-G domains I and III, whereas the second site is not supported by cryo-EM density (**supp. Fig. S7**). After our analysis had been completed, the X-ray structure of EF-G•GDP•FA bound to the POST 70S ribosome became available[1] identifying the same binding site for FA on EF-G. Together with the recent visualisation of kirromycin[11], our analysis demonstrates that cryo-EM at sub-nanometer resolution is capable of identifying the ribosomal binding sites of antibiotics.

FA stabilizes the rotated state of domain III thereby preventing the conformational change of EF-G to the GDP state and the subsequent dissociation of EF-G from the ribosome. In this sense, there is some parallelism between the action of FA and the stalling of EF-Tu by kirromycin[3,11]. However, unlike kirromycin, ribosome binding of EF-G appears to be required for FA binding because in the presence of FA several GTPase cycles of EF-G can occur before the drug stalls the factor on the ribosome[14]. Because the binding site for FA is created by the ribosome-driven rotation of domain III of EF-G and because the switch I of EF-G in the GTP conformation shields the FA binding site, there is probably only a short time window during the EF-G cycle during which the drug can successfully bind. It is interesting that FA acts analogous to the anti-fungal antibiotic sordarin. Sordarin also targets the active, ribosome-induced conformation of eEF2 and stabilizes the rotated position of domain III, albeit from a distinct binding site located between domains III, IV and V[15,16].

Intermediate states of tRNA translocation with superimposed A-tRNA

During translocation two tRNAs are moved from the A- and P-sites to the P- and E-sites respectively. Thus, authentic translocation intermediates contain two tRNAs. However, despite considerable effort[7,17-19], it has been possible so far to obtain direct structural information about EF-G•70S complexes with two tRNAs only when the complex was in the POST state with a non-ratcheted ribosome and tRNAs are present in classical P/P- and E/E-sites (e.g. the recent X-ray structure[1]). Therefore, structural insights into intermediate states of translocation, i.e. ratcheted ribosomal EF-G complexes, have utilised complexes without an A-site peptidyl-tRNA[7-9], since at least an anticodon stem-loop bound to the A-site is

required to complete translocation[20]. Such complexes appear to be valid model for translocation intermediates as EF-G binding and GTPase activity are hardly influenced by the absence of the A-tRNA[21,22].

Nevertheless, it is important to consider, if the conclusions for translocation intermediates can be extrapolated to an authentic complex containing two tRNAs. In the case of our TI[POST] this is possible, because the head swivel and the back-rotation of the body/platform leads to a juxtaposition of the ribosomal residues of the head that contact A-tRNA and ribosomal residues of the body that contact P-tRNA (**Fig. 2b**). Thus in addition to the observed pe/E site a potential ap/P site is formed. Moreover, in the TI[POST] the distance between the tip of domain IV of EF-G and the pe/E tRNA is ~27 Å - similar to the equivalent distance of 31 Å between EF-G and the E/E tRNA as observed in the POST EF-G•70S complex[1] that accommodates an additional intervening P/P tRNA. Thus, a second tRNA occupying a hypothetical ap/P position can be superimposed into the TI[POST] without steric interference with the binding position of EF-G (**supp. Fig. S6a**). In contrast, inclusion of a second tRNA in a hypothetical A/P hybrid state in the TI[PRE] is incompatible with the observed location of domain IV of EF-G, which is positioned in the decoding region. However, the ribosome conformation of the TI[PRE] as well as the position of the pp/E tRNA is corroborated by the strong similarity with the rotated sub-state of the PRE complex. Thus, we consider it possible that domain IV of EF-G is repositioned in the TI[PRE] and that in the transient initial binding mode EF-G adopts a more closed conformation. It is also possible that the A-tRNA is moved more towards the P/E tRNA. The distance between the tip of domain IV of EF-G and the pp/E tRNA is 19 Å and this is could be still large enough to place a second tRNA inbetween without major steric clashes (**supp. Fig. S6b**). Structures of translocation intermediates with two tRNAs will be necessary to validate these predictions.

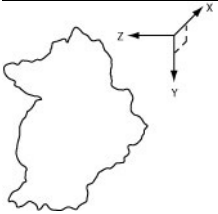**Translocation intermediates and the role of GTP hydrolysis**

Spontaneous ribosomal inter-subunit rotation and tRNA hybrid site formation within the PRE complex has been suggested to be a reflection of an energy landscape that allows sampling of several metastable conformations for a defined ribosomal complex[23]. We have shown here that the 70S•EF-G•GDP•FA complex and also the 70S•EF-G•GMPPNP complex (**supp. Fig. S5; supp. Table 1**) exist in at least two major sub-states, i.e. the TI[PRE] and TI[POST]. Therefore, our findings here provide supportive evidence for the emerging energy landscape model of ribosomal function and show that ratcheted 70S•EF-G complexes exhibit intrinsic conformational heterogeneity as well. Although the sub-states of the 70S•EF-G•GMPPNP complex are generally similar to the sub-states of the 70S•EF-G•GDP•FA complex (**supp. Fig. S5; supp. Table 1**), there is an interesting difference in the relative population of both states. The majority of ribosomes in the 70S•EF-G complex stalled using a

non-hydrolyzable GTP analogue are in the TI^{PRE}, whereas in the 70S•EF-G complex stalled using GTP and fusidic acid (FA), the TI^{POST} dominates.

It was noted early on that FA-stalled complexes show a smaller ratchet-like subunit rearrangement than GMPPNP-stalled complexes[8]. Our observation is in overall agreement with these previous single-particle reconstructions as the 4° intersubunit rotation of the TI^{POST} dominating the FA-stalled complex is smaller than the 7° intersubunit rotation of the TI^{PRE} dominating the GMPPNP-stalled complex (**supp. Table 1**). Apparently, there are subtle differences in the interaction of EF-G•GMPPNP and EF-G•GDP•FA with the ribosome, respectively, that influence the energy landscape of the ribosome, although at the present resolution the overall EF-G conformation appears to be very similar. We are therefore tempted to speculate that the GTPase reaction of EF-G followed by release of Pi leads to a preference of the TI^{POST} over the TI^{PRE}. This would be in agreement with the finding that release of Pi and $tRNA_2$-mRNA translocation have been shown to be much slower than GTP hydrolysis [24]. Furthermore, the putative influence of GTP hydrolysis/Pi release on the energy landscape of the ribosome provides a structural explanation for the acceleration of tRNA translocation by GTP hydrolysis[25]. We previously suggested that a network of interactions between the rotated 30S subunit and the γ-phosphate of GTP, *via* domain III of EF-G and its ordered switch I region, stabilizes the rotated conformation of the ribosome[9]. Accordingly, flipping-out of the switch I region upon GTP hydrolysis[10] will reduce the stabilization effect on the rotated 70S conformation, as seen in the TI^{PRE}, and will allow reverse-rotation of the 30S subunit to the partially ratcheted state, as seen in the TI^{POST}. Ultimately, regardless of the timing of release of Pi, the loss of the γ-phosphate allows EF-G to adopt the low affinity GDP state, which dissociates from the POST state ribosome.

Supplemental Table 1

Table 1: Quantification of ribosomal intersubunit rotation and head swiveling

	body/platform (global rotation *versus* 50S subunit)	head (global rotation versus 50S subunit)	head (swivel movement relative to 30S body)
T. thermophilus 70S•EF-G•GDP•FA TI[PRE]	7° 6° / -3° / 1° *0.73 / 0.87*	11° 8° / -6° / 2° *0.38 / 0.89*	5° 1° /-3° / 2°
T. thermophilus 70S•EF-G•GDP•FA TI[POST]	4° 3° / -3° / 1° *0.80 / 0.87*	21° 2° / -17° / 10° *0.65 / 0.82*	18° 3° / -9° / 6°
T. thermophilus 70S•EF-G• GMPPNP TI[PRE]	7° 6° / -3° / 1° *0.71 / 0.84*	11° 8° / -8° / 2° *0.66 / 0.85*	5° 1° / -5° / 2°
T. thermophilus 70S•EF-G• GMPPNP TI[POST]	5° 3° / -3° / 1° *0.80 / 0.86*	19° 6° / -13° / 7° *0.69 / 0.80*	15° 4° / -5° / 4°
E. coli EMDB-1540[a] PRE (classical)	2° 0° / 0° / 0° *n.d.*	2° 0° / 0° / 0° *n.d.*	2° 0° / 0° / 0°
E. coli EMDB-1541[a] PRE (rotated)	8° 6° / -4° / 1° *n.d.*	10° 7° / -3° / 1° *n.d.*	3° 0° / 0° / 0°

The rotational parameters required aligning the entire 30S head, or body/platform domains to the same feature in the 70S-fMet-tRNA complex[26] were calculated after the various structures were aligned based on their 50S subunits. The coordinate system is the same as in previous comparisons[9,15,27]. The angle in the upper row is the maximal rotation angle determined in UCSF Chimera with the *fit in map* tool. The angles in the middle row, $\alpha/\beta/\gamma$, are determined with SPIDER and describe rotations around the x-, y- and z-axis, as defined in the cartoon outline of the 30S subunit. The values given describe the transformation from the 70S-fMet-tRNA reference structure to the indicated structures. The values in the lower row (Italics) are the respective cross-correlation coefficient before/after alignment.

[a] Orientation parameters for the spontaneous inter-subunit rotation of the *E. coli* PRE complex[28] were calculated using maps deposited in the EM database (identifiers EMDB-1540 and EMDB-1541) after adjustment of the scale.

Supplemental Figure legends

Supp. Fig. S1: Multi-particle refinement strategy

Multi-particle refinement[11,17,29] was used to account for conformational heterogeneity of the *T. thermophilus* 70S•EF-G•GDP•FA complex. Initially, the data set was sorted into up to six subpopulations. After a first phase of multiparticle refinement, we obtained a major population of particle images (52 %; 303,665). Although the corresponding structure had strong EF-G density, limited resolution pointed to conformational heterogeneity of the data set. Therefore, we proceeded with the second phase of multiparticle refinement, leading to a further subdivision of the subset obtained in the first phase into two major populations of particle images (27 % and 19 % of the complete data set, respectively). Each was subsequently refined individually to yield the two final maps at 7.6 and 7.8 Å resolution, respectively. The resulting cryo-EM maps of the ribosomal complexes are shown in side views. Numbers and percentages indicate total particle projections and fractions of the whole data set, respectively.

Supp. Fig. S2: Resolution curves of the TI^{PRE} and TI^{POST} complexes

The resolution curves of cryo-EM maps of the TI^{PRE} (red) and the TI^{POST} (green) are shown. The standard FSC curves (solid lines) indicate that the resolution of the TI^{PRE} (red) and the TI^{POST} based on the 0.5 FSC cut-off, is 7.8 Å and 7.6 Å, respectively. FSC curves between the cryo-EM maps and density derived from the pseudo-atomic models (dashed lines) show that the agreement between the maps and the models is in the same order as the nominal resolution.

Supp. Fig. S3: Cryo-EM reconstructions of sub-states I (TI^{PRE}) and II (TI^{POST}) of the 70S•EF-G•GDP•FA complex

a,b, The cryo-EM maps of sub-state I (TI^{PRE}) (a) and sub-state II (TI^{PRE}) (b) of the 70S•EF-G•GDP•FA complex are shown from the L7-stalk-site. The ribosomal 30S subunit is marked yellow, the 50S subunit blue, EF-G red and the tRNA green.

c, Comparison of sub-states I and II of the 30S with the maps aligned at the 50S subunit indicating the difference in terms of ratcheting and **d,** aligned at the body/platform domains of the 30S subunit highlighting differences in head swiveling. The 30S of sub-state I (TI^{PRE}) is rendered in transparent orange, while the 30S of sub-state II (TI^{POST}) is in solid yellow.

Supp. Fig. S4: Comparison of TI^PRE (sub-states I) and TI^POST (sub-states II) of the 70S•EF-G•GDP•FA complex

a, b, Comparative molecular models of 30S (a) and 50S (b) subunits in the TI^PRE (sub-state I) and TI^POST (sub-state II) conformation, represented in ribbon mode. Color code: 30S TI^PRE, green; 30S TI^POST, yellow; 50S TI^PRE, blue; 30S TI^POST, magenta. Arrows highlight the inter-subunit rotation, the head swivel (a) and the movement of the L1 protuberance (b).

Supp. Fig. S5: Cryo-EM reconstructions of sub-states I and II of the 70S•EF-G•GMPPNP complex

a,b, The cryo-EM maps of sub-state I (TI^PRE) (a) and sub-state II (TI^PRE) (b) of the 70S•EF-G•GMPPNP complex are shown from the 30S. The ribosomal 30S subunit is marked yellow, the 50S subunit blue, EF-G red and the tRNA green.
c, Comparison of sub-states I and II of the 30S with the maps aligned at the 50S subunit indicating the difference in degrees of ratcheting. The 30S of sub-state I (TI^PRE) is in solid yellow, while the 30S of sub-state II (TI^POST) is rendered in transparent orange.
d, Comparison of sub-state I (TI^PRE) of the 70S•EF-G•GMPPNP complex (transparent yellow) with sub-state I (TI^PRE) of the 70S•EF-G•GDP•FA complex (grey) indicating the overall similarity between the TI^PRE sub-states..

Supp. Fig. S6: Docking of a second tRNA into TI^PRE and TI^POST

a,b, Close-up on the decoding region of the 30S subunit showing the relative positions of domain IV of EF-G and the tRNA binding sites. The surfaces of TI^POST (a) and TI^PRE (b) are transparent with molecular models in ribbons representation (30S subunit, yellow; EF-G, red). In (a) the pe/E-tRNA is coloured orange and the superposition of an ap/P-tRNA is green, whereas in (b) the P/E-tRNA is coloured green and the superposition of an A/P-tRNA is blue. The tRNA had to be shifted from the decoding center of the A-site towards the P/E tRNA in order to avoid overlap with domain IV of EF-G. Note the close proximity between domain IV of EF-G and the A/P-tRNA in (b), whereas in (a) there is no steric clash between domain IV of EF-G and the ap/P-tRNA.

Supp. Fig. S7: The structure of EF-G and the fusidic acid (FA) binding site

The molecular model for MDFIT docked EF-G (red ribbon) is shown superposed with the corresponding region of the cryo-EM density maps (black mesh). FA is in cyan, GDP in magenta.

a, Result of the Ligsite search[13] indicating the two most likely ligand binding sites (shown as yellow balls) for a small molecule such as FA. The analysis of binding pockets yields the same results for the TI^{PRE} and TI^{POST}.

b, The inset shows a close-up view of the two ligands present in the EF-G structure in the TI^{POST} state. Nearby residues known to be important for binding of FA[4,12] are labelled.

c,d, Comparison of the structure of ribosome-bound EF-G for the TI^{PRE} (c) and TI^{POST} (d).

Supplemental Movie 1:

The animation compares the cryo-EM maps of sub-state I (TI^{PRE}) and sub-state II (TI^{POST}) of the 70S•EF-G•GDP•FA complex, which are shown as mesh superposed with docked molecular models in ribbons representation (see also legend to **Fig. 1**): EF-G (red), the tRNA (green), the 16S rRNA (yellow), and the 30S ribosomal proteins (pink). The maps are shown from the 50S side with the 50S subunit computationally removed. Alignment was based on the respective 50S subunits.

Supplemental Movie 2:

The animation compares the cryo-EM maps of sub-state I (TI^{PRE}) and sub-state II (TI^{POST}) of the 70S•EF-G•GDP•FA complex, which are shown as mesh superposed with docked molecular models in ribbons representation (see also legend to **Fig. 1**): EF-G (red), the tRNA (green), the 16S rRNA (yellow), and the 30S ribosomal proteins (pink). The maps are shown as a top view onto the 30S subunit with the 50S subunit computationally removed. Alignment was based on the respective 50S subunits.

Supplemental Movie 3:

The animation compares the molecular models of sub-state I (TI^{PRE}) and sub-state II (TI^{POST}) of the 70S•EF-G•GDP•FA complex in a close-up of the tRNA binding. The 30S subunit is shown with yellow ribbons, the tRNAs as blue ribbons and ribosomal residues that contact tRNAs in A-, P- and E-sites as spheres coloured magenta, green and orange, respectively (see also **Fig. 2a, b**).
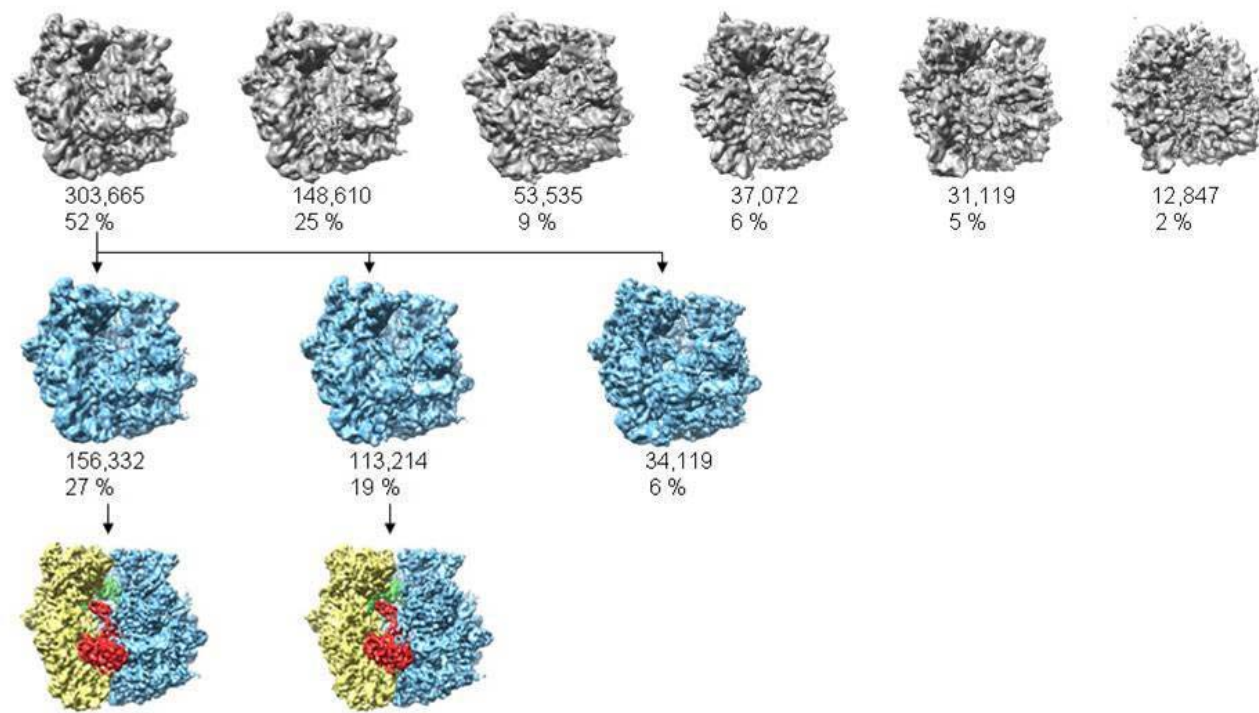

Supplemental Movie 4:

In a common 50S alignment, the P/E-tRNA (green ribbon) of TI^{PRE} (sub-state I) and the pe/E-tRNA (magenta ribbon) of TI^{POST} (sub-state II) together with their respective mRNA codons

are compared to the positions of the tRNAs in classical A-, P- and E-sites and the mRNA (grey ribbons). See also Fig. 3d.
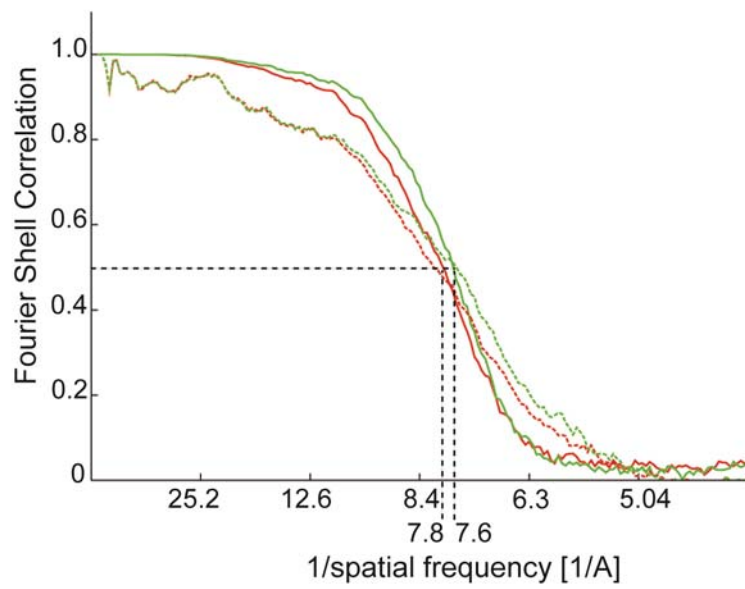

Supplemental References

[1]   Gao, Y. G. et al., The structure of the ribosome with elongation factor G trapped in the posttranslocational state. *Science* 326, 694 (2009).

[2]   Selmer, M. et al., Structure of the 70S ribosome complexed with mRNA and tRNA. *Science* 313, 1935 (2006).

[3]   Schmeing, T. M. et al., The crystal structure of the ribosome bound to EF-Tu and aminoacyl-tRNA. *Science* 326, 688 (2009).

[4]   Laurberg, M. et al., Structure of a mutant EF-G reveals domain III and possibly the fusidic acid binding site. *J.Mol.Biol.* 303, 593 (2000).

[5]   A, A. Evarsson et al., Three-dimensional structure of the ribosomal translocase: elongation factor G from Thermus thermophilus. *Embo J* 13, 3669 (1994).

[6]   Czworkowski, J., Wang, J., Steitz, T. A., and Moore, P. B., The crystal structure of elongation factor G complexed with GDP, at 2.7 A resolution. *Embo J* 13, 3661 (1994).

[7]   Valle, M. et al., Locking and unlocking of ribosomal motions. *Cell* 114, 123 (2003).

[8]   Frank, J. and Agrawal, R.K., A ratchet-like inter-subunit reorganization of the ribosome during translocation. *Nature* 406, 318 (2000).

[9]   Connell, S. R. et al., Structural basis for interaction of the ribosome with the switch regions of GTP-bound elongation factors. *Mol Cell* 25, 751 (2007).

[10]   Ticu, C. et al., Conformational changes in switch I of EF-G drive its directional cycling on and off the ribosome. *EMBO J* 28, 2053 (2009).

[11]   Schuette, J. C. et al., GTPase activation of elongation factor EF-Tu by the ribosome during decoding. *EMBO J* 28, 755 (2009).

[12]   Hansson, S. et al., Structural insights into fusidic acid resistance and sensitivity in EF-G. *J Mol Biol* 348, 939 (2005).

[13]   Huang, B. and Schroeder, M., LIGSITEcsc: predicting ligand binding sites using the Connolly surface and degree of conservation. *BMC Struct Biol* 6, 19 (2006).

[14]   Seo, H. S. et al., EF-G-dependent GTPase on the ribosome. conformational change and fusidic acid inhibition. *Biochemistry* 45, 2504 (2006).

[15]   Spahn, C. M. et al., Domain movements of elongation factor eEF2 and the eukaryotic 80S ribosome facilitate tRNA translocation. *EMBO J* 23, 1008 (2004).

[16]   Jorgensen, R. et al., Two crystal structures demonstrate large conformational changes in the eukaryotic ribosomal translocase. *Nat Struct Biol* 10, 379 (2003).

[17]   Penczek, P. A., Frank, J., and Spahn, C. M., A method of focused classification, based on the bootstrap 3D variance analysis, and its application to EF-G-dependent translocation. *J Struct Biol* 154, 184 (2006).

[18]   Agrawal, R.K. et al., EF-G-dependent GTP hydrolysis induces translocation accompanied by large conformational changes in the 70S ribosome. *Nature Struct.Biology.* 6, 643 (1999).

[19]   Scheres, S. H. et al., Disentangling conformational states of macromolecules in 3D-EM through likelihood optimization. *Nat Methods* 4, 27 (2007).

[20]   Joseph, S. and Noller, H.F., EF-G-catalyzed translocation of anticodon stem-loop analogs of transfer RNA in the ribosome. *EMBO Journal* 17, 3478 (1998).

[21]   Rodnina, M. V., Savelsbergh, A., Katunin, V. I., and Wintermeyer, W., Hydrolysis of GTP by elongation factor G drives tRNA movement on the ribosome. *Nature* 385, 37 (1997).
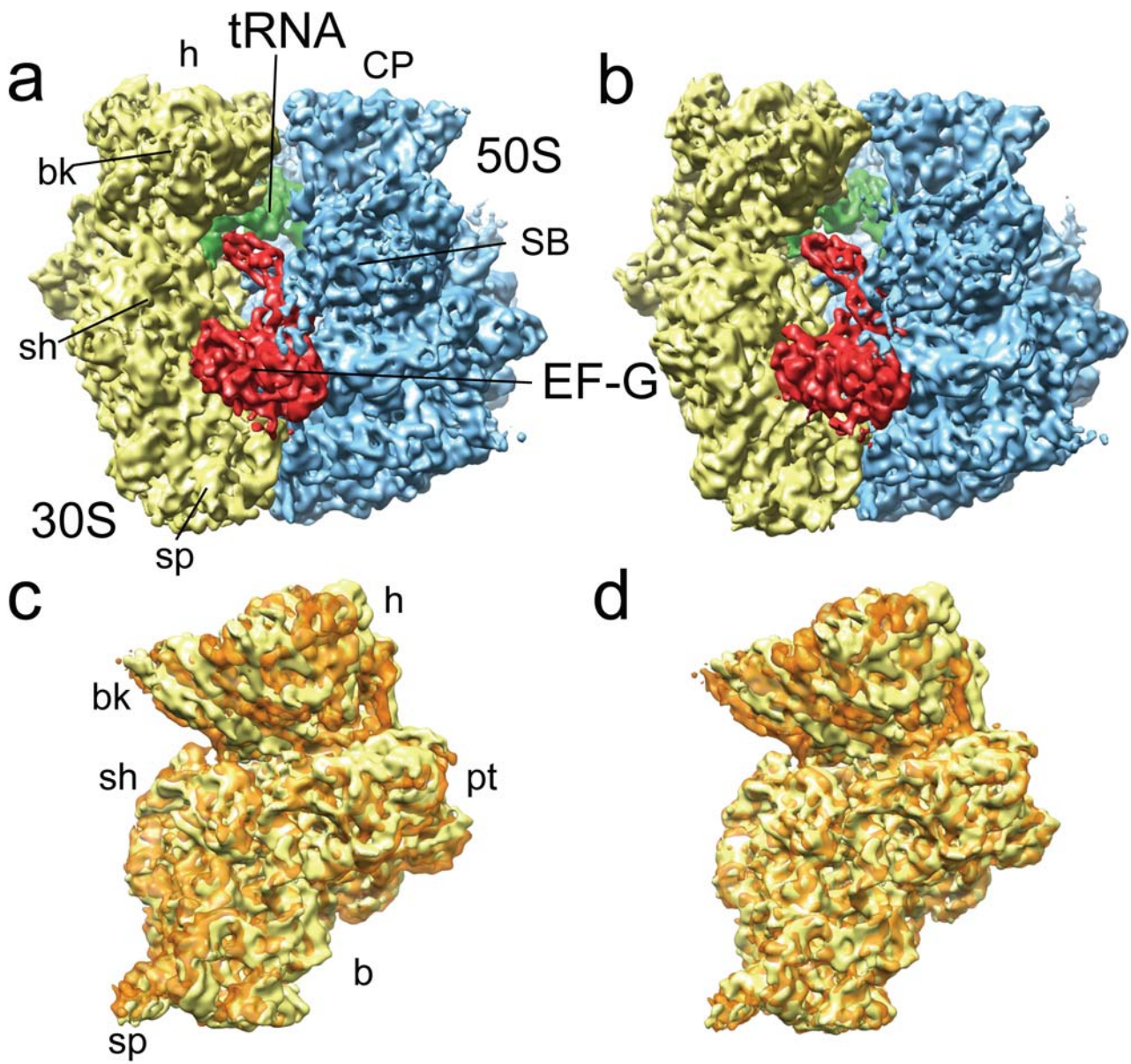
[22] Wilden, B., Savelsbergh, A., Rodnina, M. V., and Wintermeyer, W., Role and timing of GTP binding and hydrolysis during EF-G-dependent tRNA translocation on the ribosome. *Proc Natl Acad Sci U S A* 103, 13670 (2006).

[23] Munro, J. B., Sanbonmatsu, K. Y., Spahn, C. M., and Blanchard, S. C., Navigating the ribosome's metastable energy landscape. *Trends Biochem Sci* 34, 390 (2009).

[24] Rodnina, M., Savelsbergh, A., Katunin, V.I., and Wintermeyer, W., Hydrolysis of GTP by elongation factor G drives tRNA movement on the ribosome. *Nature* 385, 37 (1997).

[25] Savelsbergh, A. et al., An elongation factor G-induced ribosome rearrangement precedes tRNA-mRNA translocation. *Mol Cell* 11, 1517 (2003).

[26] Gabashvili, I.S. et al., Solution structure of the *E. coli* 70S ribosome at 11.5 Å resolution. *Cell* 100, 537 (2000).

[27] Spahn, C. M. et al., Localization of the ribosomal protection protein Tet(O) on the ribosome and the mechanism of tetracycline resistance. *Mol Cell* 7, 1037 (2001).

[28] Agirrezabala, X. et al., Visualization of the hybrid state of tRNA binding promoted by spontaneous ratcheting of the ribosome. *Mol Cell* 32, 190 (2008).

[29] Spahn, C. M. and Penczek, P. A., Exploring conformational modes of macromolecular assemblies by multiparticle cryo-EM. *Curr Opin Struct Biol* 19, 623 (2009).
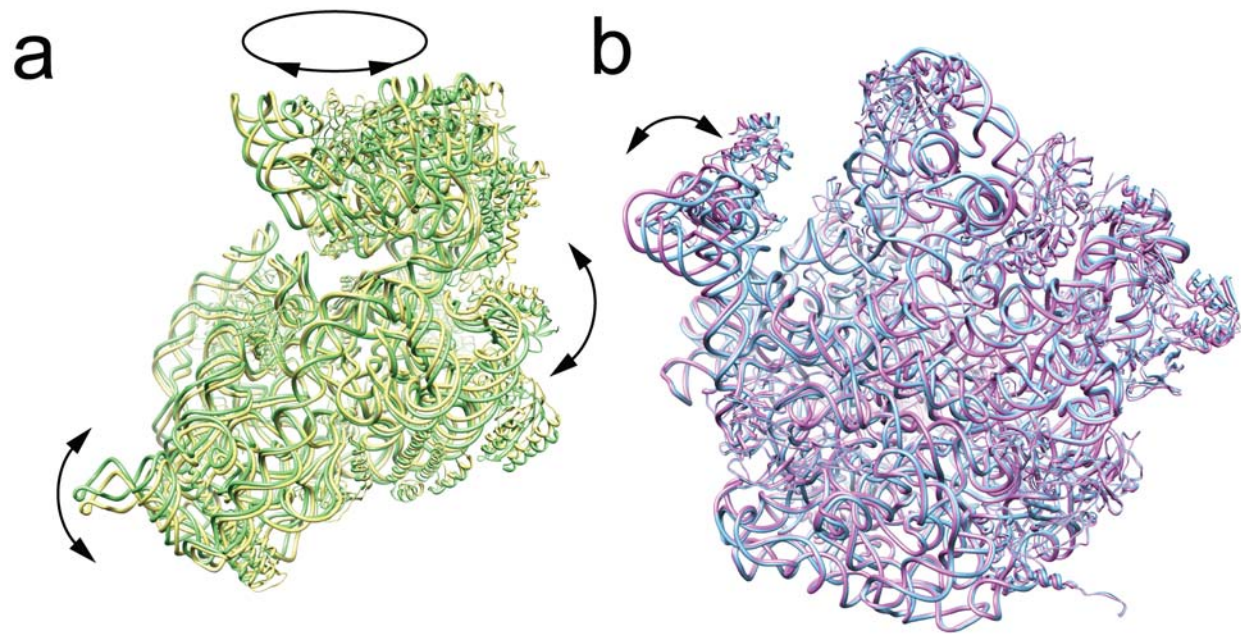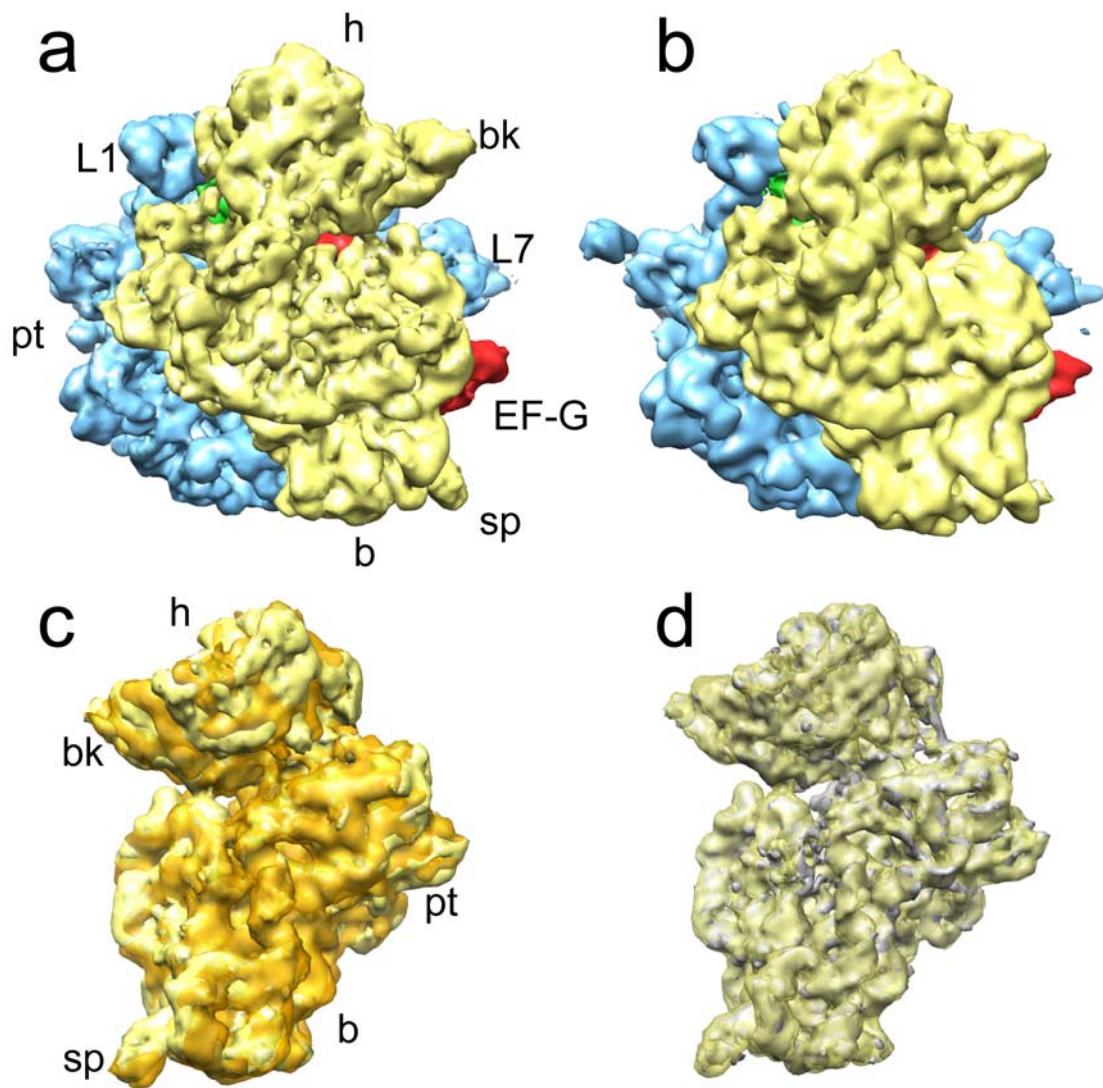
303,665
52 %

148,610
25 %

53,535
9 %

37,072
6 %

31,119
5 %

12,847
2 %

156,332
27 %

113,214
19 %

34,119
6 %

Supplemental Figure S1

Supplemental Figure S2

a h tRNA CP
bk
SB
sh
EF-G
50S
30S
sp

b

c h
bk
sh pt
b
sp

d

Supplemental Figure S3

a

b
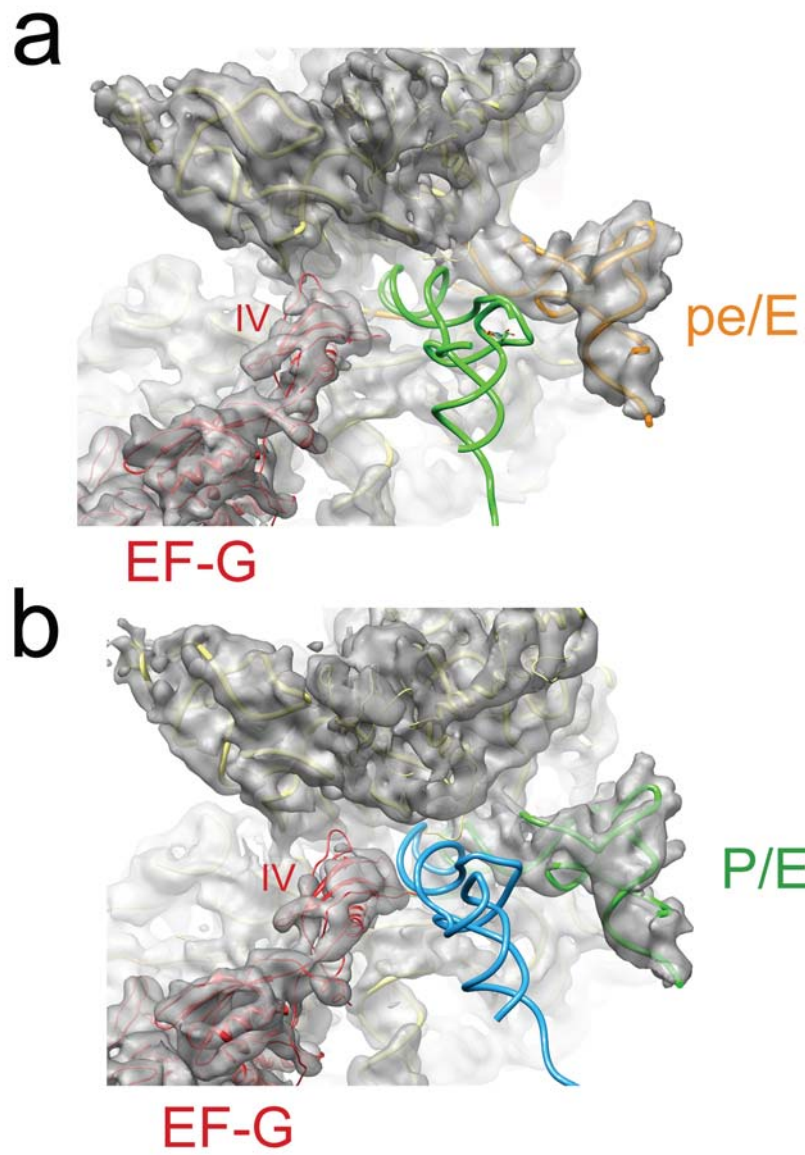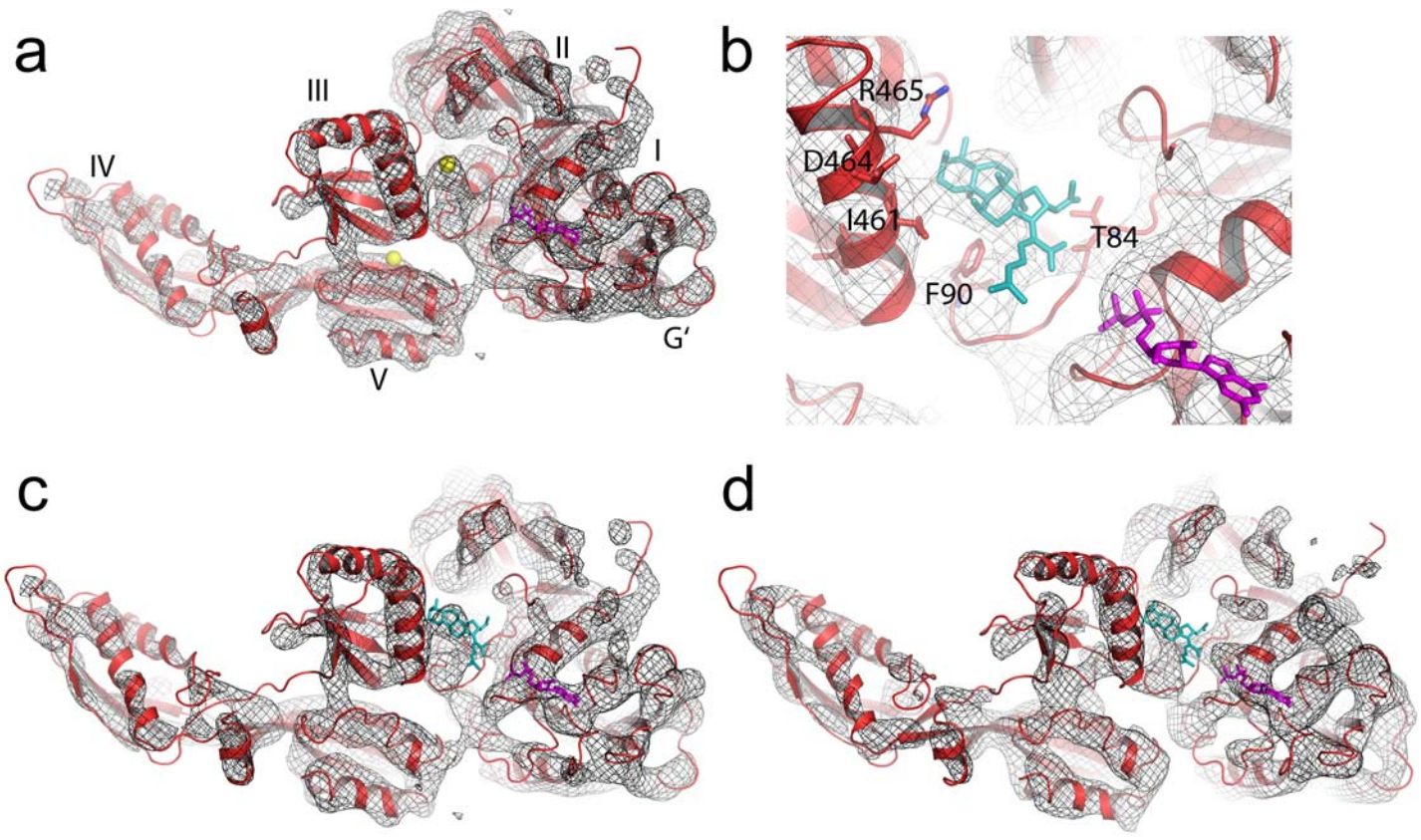
Supplemental Figure S4

Supplemental Figure S5

Supplemental Figure S6

Supplemental figure S7